

Some aspects on the mechanical analysis of micro-shutters

Rainer K. Fettig^a, Jonathan L. Kuhn^b, S. Harvey Moseley^b, Alexander S. Kuttyrev^a,
Jon Orloff^c, and Shude Lu^c

^aRaytheon ITSS, Greenbelt, MD

^bNASA/Goddard Space Flight Center, Greenbelt, MD

^cDepartment of Electrical Engineering, University of Maryland
College Park, MD

ABSTRACT

An array of individually addressable micro-shutters is being designed for spectroscopic applications. Details of the design are presented in a companion paper. The mechanical design of a single shutter element has been completed. This design consists of a shutter blade suspended on a torsion beam manufactured out of single crystal silicon membranes. During operation the shutter blade will be rotated by 90 degrees out of the array plane. Thus, the stability and durability of the beams are crucial for the reliability of the devices. Structures were fabricated using focused ion beam milling in a FEI 620 dual beam machine, and subsequent testing was completed using the same platform. This allowed for short turn around times. We performed torsion and bending experiments to determine key characteristics of the membrane material. Results of measurements on prototype shutters were compared with the predictions of the numerical models. The data from these focused studies were used in conjunction with experiments and numerical models of shutter prototypes to optimize the design. In this work, we present the results of the material studies, and assess the mechanical performance of the resulting design.

Keywords: micro-shutter, stiffness, strength, fracture, design, analysis

1. INTRODUCTION

The advent of micro electro mechanical systems (MEMS) technology has spurred development of arrays of individually controlled active elements. The devices can independently control the paths of rays of light. While the majority of researchers have focused on reflective micro-mirror arrays, transmissive designs provide much lower scattered light and therefore higher contrast. As a result, Moseley et. al.¹ developed a micro-shutter array design, which functions as an actively controlled mask for astronomical applications. A specific example includes the near infrared Multi-Object Spectrometer (MOS) proposed for the Next Generation Space Telescope (NGST). In this case, the operating temperature of the instrument is 30K.

The proposed mask design consists of a 1000 by 1000 array of transmissive micro-shutters with a fill factor of 80%. Each shutter consists of a 100 by 100 μm blade suspended from torsion beams parallel to one blade edge. The primary load sustained by each shutter is induced by a 90 degree out of plane rotation of the blade. The details of the system mechanics are presented in a companion paper.¹ The focus of this work is on the design and analysis of a single shutter.

Our objective is to complete practical and rapid design iterations of a single shutter element as shown in Fig. 1. Test structures were fabricated using focused ion beam milling in a FEI 620 dual beam machine. This platform allows for the manufacture and test of numerous shutter designs in as little as an afternoon. The approach results in short trial and error turn around times, which are currently essential in MEMS design. However, even with such rapid fabrication iterations, an efficient design process will be driven by intelligent selection of base geometry and dimensions. Ultimately, the mechanical response of the design in service must also be understood to ensure reliable performance.

In this work, key aspects of the design of a micro-shutter are addressed through simplified numerical, analytical, and experimental techniques. Emphasis is placed on characterizing the material stiffness and strength. This data is used in turn to develop a correlated finite element model of the micro-shutter, which is used to optimize the design.

Send correspondence to R.K.F. E-mail: rfettig@stx.com

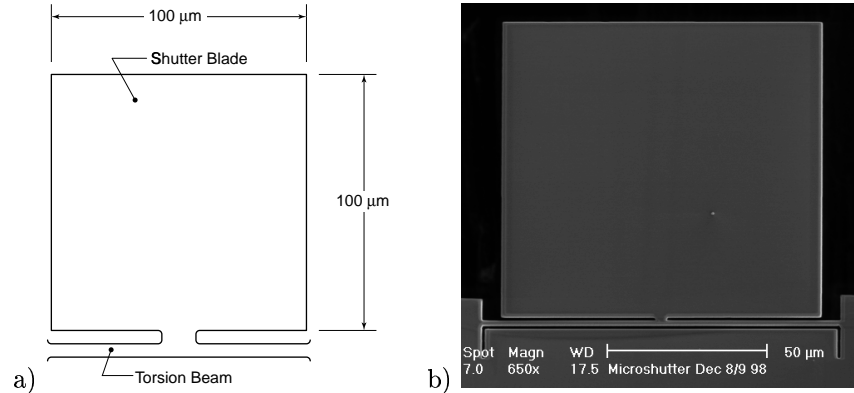


Figure 1. a) Schematic of the basic shutter design. b) Scanning electron micro-graph of a micro-machined shutter.

2. MICRO-SHUTTER DEVELOPMENT

Accurate mechanical analysis relies on accurate descriptions of the material properties, geometry, and boundary conditions. After a relatively long and thorough history of research, Schweitz and Ericson² conclude that the elastic properties of micro machined materials equal the bulk elastic properties for the same material measured macroscopically. In fact, bulk elastic property measurements completed using established macroscopic testing techniques tend to be more reliable. On the other hand, Schweitz and Ericson also conclude that the material strength does depend on the structure size, shape, and processing. The latter conclusion is consistent with brittle fracture theory.

As a result, we may use tabulated bulk elastic properties for mechanical design and analysis if they are available. However, the material strength should be determined experimentally for each design by using test elements that are similar in size, shape, and processing to the particular design structure under study. As indicated by Schweitz and Ericson, the Weibull³ probability distribution function gives the most accurate description of the brittle material strength. This approach accounts for the scatter that is common in brittle material strengths. The Weibull method requires a large number (100 or more) of tests to establish statistical confidence. As a result, we initially use the minimum strength of a small number of samples as a first order approximation for the purpose of preliminary design studies. Final analysis for flight qualification must be based on tests of a full spectrum of samples.

In the next section, the experimental technique is outlined, followed by the material stiffness and strength test results. Subsequently, we present preliminary results of the micro-shutter design.

2.1. Materials and Experimental Techniques

Our shutter concept is based on the idea that essentially one homogeneous layer of high strength material is patterned during processing and used as a mechanically active layer, as opposed to multiple layer deposition and structuring processes as used for most MEMS devices. To perform the material and design test described in this paper, two types of layers were examined. Both were prepared as free-standing membranes suspended on anisotropically etched (KOH) silicon substrates. One type of layer was single crystalline silicon of nominal $2 \mu m$ thickness prepared as a silicon on silicon oxide layer. The membrane has a one sided Chromium layer of about $20 nm$. The second type was a low stress nitride layer of about $0.5 \mu m$ with a one side Aluminum layer of about $20 nm$.

All experiments were performed in an FEI 620 focused ion beam milling machine. The FEI 620 is a dual beam machine, with an ion and electron column, which allows ion milling and *in situ* scanning electron microscopy. Ion milling can be performed with ion beam spot sizes of $20 nm$ to $1 \mu m$ and machining rates in silicon up to $10 \mu m^3/s$. The machine is also equipped with a micro-manipulator needle and the possibility to deposit platinum by ion induced metal organic chemical vapor deposition (MOCVD). This combination turned out to be a perfect tool for a variety of experimental techniques to:

- machine and observe structures.
- perform bending and moving tests, using the manipulator needle.

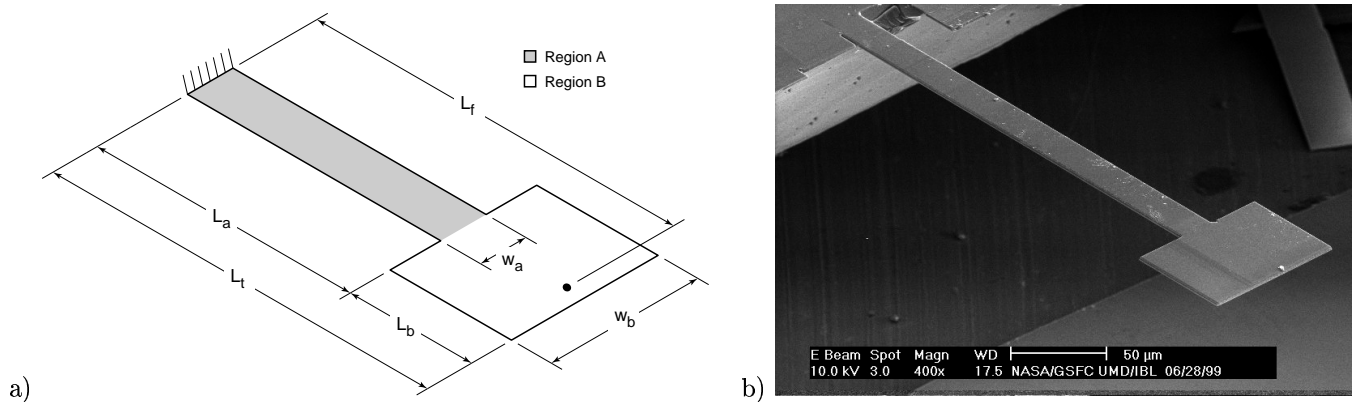


Figure 2. a) Schematic drawing of the cantilever beam vibration test specimen. b) Scanning electron micro-graph of machined cantilever beam.

- analyze time response to a needle induced force. This is accomplished by focusing the electron beam spot on a moving object, and observing the secondary electron time signal.
- machine electrodes, weld them to a needle through platinum deposition and use them to apply electrical forces to a machined micro-structure.
- machine MEMS structures, weld them to a needle and use them.

Three studies were conducted using the membranes and the above procedures. First, we measured the membrane Young's modulus using a cantilever beam vibration test. The strengths of the materials were measured using a cantilever structure with thickness and width similar to the micro-shutter torsion bar dimensions. Lastly, we fabricated shutters and rotated them as much as 180 degrees. Complimentary analytical and numerical studies were used as needed to compute the stiffness, strength, and stresses from the experimental results. Finite element analysis was completed using ANSYS⁴ on a Sun Microsystems Sparc workstation. Details of these studies are presented in the following sections.

2.2. Material Stiffness

Some researchers⁵⁻⁷ used bending tests to determine the stiffness and fracture strength of silicon membranes. In these cases the membranes were more than 10 μm thick. Forces greater than .01 Newtons induced reasonable bending and failure. The membranes used in this study are 2 and .5 μm thick. The corresponding forces are significantly smaller than 0.01 Newtons. Currently available force transducers can not resolve forces at such a low magnitude. As a result we have used a vibration test method to determine the Young's modulus.

In the vibration test, the ion beam is used to fabricate long cantilever beams of total length L_t in a "T" shape as shown in Fig. 2. At the fixed end, the beam has a narrow width w_a , which extends to a length L_a . The remaining portion of the beam of length L_b is wider with width w_b . The total length is denoted as $L_t = L_a + L_b$, and is aligned with the $\langle 110 \rangle$ crystalline direction. The purpose of this configuration is to yield a cantilever mass/spring system, whose first natural frequency can be measured and computed analytically. In particular, the mass at the end can be increased to reduce the frequency to a range that can be easily measured.

In the experimental setup, the beam is pushed vertically with a needle and released. The approximate natural frequency is measured as described above. Subsequently, an electrode is placed in close proximity to the end of the beam and a periodic voltage is applied. The frequency of the voltage is varied over a small range around the approximate value previously determined. The response is monitored, and the frequency of peak displacement is recorded.

The natural frequency of a cantilever spring mass system can be expressed as^{8,9}

$$f = \frac{1}{2\pi} \sqrt{\frac{3EI}{L^3(m_b + C_1 m_a)}} \quad (1)$$

where the constant C_1 equals 0.2357, f is the cyclic natural frequency in Hz, $L = L_a + L_b/2$ is the cantilever length to the center of the end mass, E is the Young's modulus, $m_a = \rho w_a t L_a$ is the mass of region A, and $m_b = \rho w_b t L_b$ is the mass of region B, where ρ is the mass density. The area moment of inertia I equals $(w_a t^3)/12$, where w_a is the region A width, and t is the membrane thickness.

In order to validate the above equation for the "T" shape beam, the predicted frequency was compared with results from an ANSYS finite element model for silicon. The finite element model was comprised of shell elements with $L_a = 250 \mu m$, $w_a = 20 \mu m$, $L_b = 80 \mu m$, $w_b = 70 \mu m$, and thickness $t = 2.45 \mu m$. A Young's modulus of $E = 176$ GPa was selected from Ref. 10 for the $\langle 110 \rangle$ direction. The first mode frequency was calculated using both the finite element model ($f_{fe} = 19200$ Hz) and equation (1) ($f_{eq} = 18600$ Hz). The relative difference, $(f_{fe} - f_{eq})/f_{fe} = 0.046$, which we consider to be a reasonable approximation.

As described above, the resonant frequency is measured from the experiment for a given geometry. Hence, the Young's modulus can be isolated from the above equation, and is given by

$$E = \frac{4\pi^2 f^2 L^3 (m_b + C_1 m_a)}{3I} \quad (2)$$

which can be expanded in terms of thickness as follows

$$E = \frac{16\pi^2 f^2 L^4 \rho}{t^2} \left(\frac{w_b}{w_a} \frac{L_b}{L} + C_1 \frac{L_a}{L} \right) \quad (3)$$

A silicon cantilever beam with dimensions of $L_a = 250 \mu m$, $w_a = 20 \mu m$, $L_b = 80 \mu m$, $w_b = 70 \mu m$, and thickness $t = 1.9 \mu m$ aligned with the $\langle 110 \rangle$ crystalline direction was fabricated and tested. The natural frequency was measured as described above and determined to be $f = 12600$ Hz. Equation (3) was used to compute an effective Young's modulus of $E = 155$ GPa. This value is about 12% lower than the value of $E = 176$ GPa reported in Ref. 10.

Here we note that the Young's modulus is highly sensitive to the thickness and cross sectional shape used in the calculation. The thickness of $t = 1.9 \mu m$ was measured from scanning electron microscope images. Because the thickness t is raised to the 2nd power in equation (3) any error in t is magnified in E . We also assumed a rectangular cross sectional shape in these calculations, and in fact the shape is rounded at the corners, which will compound the error. While the chromium coating only occupies about 1% of the total volume, the modulus is significantly lower than that of silicon, and will result in a lower effective modulus. The above two sources of error combined with the potential for error introduced by using simplified equations are likely to accumulate to a total on the order of the error observed.

In a second experiment, a silicon nitride simple cantilever beam consisting of a single width w_a was fabricated and tested. The dimensions of the beam were $L_a = 205 \mu m$, $w_a = 9 \mu m$, and thickness $t = 0.55 \mu m$. The natural frequency was observed to be $f = 17800$ Hz, and the Young's modulus was calculated as $E = 220$ GPa. This value is about 43% lower than the value of $E = 385$ GPa reported in Ref. 11.

The difference in this case is much more significant than for silicon. Again the largest source of error is likely due to the thickness and cross sectional shape. The silicon nitride thickness of $0.55 \mu m$ is almost 3.5 times less than that of the silicon, but the resolution of the measurement technique is the same. Hence, the relative error introduced by the resolution limit is greater for the thinner membrane. In the case of the silicon nitride membrane, the beam width was half that of the silicon, and the corners of the cross section were observed to be more rounded. As a result the cross sectional shape error is more pronounced. Therefore, we anticipate that increased beam width will yield improved accuracy in the results.

Also, in the case of the silicon nitride membrane, the aluminum coating occupies 4% of the total volume and the relative difference between the membrane and coating moduli is more significant. The silicon nitride was fabricated using a chemical vapor deposition process which is known to result in lower density and stiffness than the bulk

properties. As a result the bulk value of $E = 385$ GPa is likely to be too high in this case. It is feasible that these sources of error may accumulate to significant differences between the experimental modulus and bulk value.

The above errors serve to confirm the conclusions of Schweitz and Ericson that micro-bending techniques are relatively inaccurate for measuring Young's modulus, and we use published values for strength studies. However, the procedure does help us to validate our experimental techniques.

2.3. Material Strength

Both silicon and silicon nitride considered for the shutter design are brittle. As such, the material strengths strongly depend on flaw distribution. The number of flaws decreases with the material volume. As a result the probability of failure also decreases and the average strength increases. At the same time, the distribution of strength may be highly scattered, which is also a function of the flaw characteristics. Scatter often increases with mean strength. Consequently, the material strength is a function of the design and processing.

Wilson et. al.⁶ presented strengths in the range of 1 – 2 GPa for micro-cantilever silicon beams with thickness of 30 μm . However, in the study presented herein, the membrane thicknesses are 2.0 and 0.5 μm , and the membranes are coated with metallic substances. These aspects will lead to strengths for the shutter design that are different than values presented elsewhere. The membranes are also so thin that simple cantilever beam tests tend to bend beyond 90 degrees before failure, making it difficult to ascertain strength.

In order to determine the material strength, we again use the "T" shaped beam shown in Fig. 2. Only in this case we select $w_b \gg w_a$ such that region B is rigid relative to region A. If we apply a vertical force F at a distance L_f from the fixed end, it is difficult to accurately measure either F or L_f . However, if we choose $L_f = nL_a$ the equations can be expressed in terms of the maximum moment $M = FL_f$ as follows.

From beam theory, the inclination θ of the end of region A (at $x = L_a$) for a vertical force F applied at a distance L_f from the fixed end is

$$\theta = \frac{F(2L_fL_a - L_a^2)}{2EI} \quad (4)$$

where L_a is the length of region A, E is the Young's modulus, and I is the cross section area moment of inertia of region A. For $L_f = nL_a$ the above equation can be rewritten as

$$\theta = \frac{FL_fL_a}{EI} \left(1 - \frac{1}{2n}\right). \quad (5)$$

The resulting maximum moment M about the fixed end of the beam is

$$M = FL_f = \frac{\theta EI}{L_a \left(1 - \frac{1}{2n}\right)}. \quad (6)$$

In the experiment we push the large blade through a rotation θ . The peak stress occurs at the fixed end and is $\sigma = Mc/I$, where c is the half thickness of the membrane. Substituting equation (6) results in

$$\sigma = \frac{\theta Ec}{L_a \left(1 - \frac{1}{2n}\right)} \quad (7)$$

The above equations become less sensitive to the force position for large n . Even for smaller $n > 2$, a small change in n has little effect on the results. Consequently, we do not need the precise location of the force L_f to get reasonably accurate measures of stress.

Equation (7) can be used to choose L_a such that the specimen will fail for small rotations. For the purpose of designing the specimen we consider the silicon membrane and pick an arbitrary failure stress $\sigma = 4$ GPa, which is double the average value of 2 GPa presented in Ref. 6. For the $\langle 110 \rangle$ direction we assume a modulus of $E = 176$ GPa, half thickness $c = 0.95 \mu m$, inclination $\theta = 10^\circ$, and scale factor $n = 10$. Solving for L_a results in a region A beam length of $L_a = 7.5 \mu m$. Therefore, a beam with this length should result in failure at relatively small rotations.

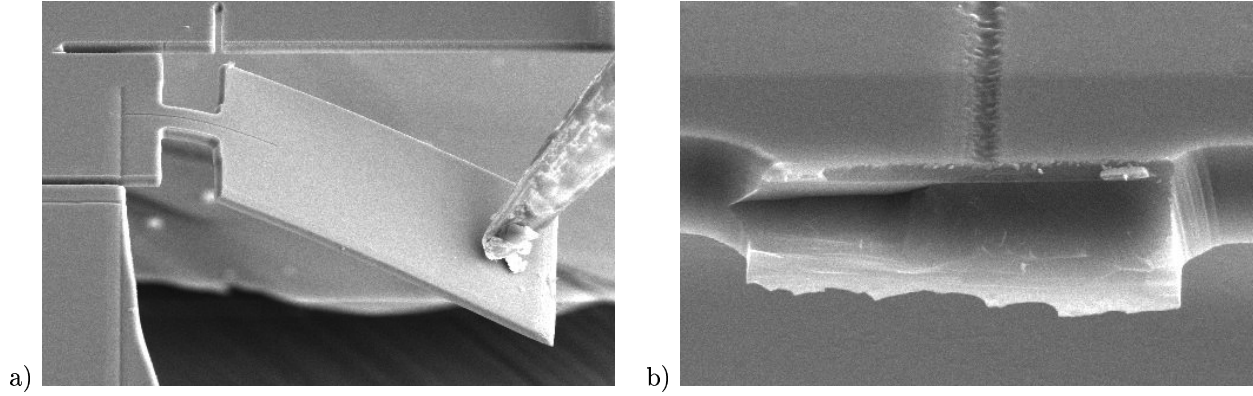


Figure 3. Scanning Electron Micrographs of a silicon “T” beam with dimensions of $L_a = 6.55 \mu m$, $w_a = 6.25 \mu m$, $L_b = 60 \mu m$, $w_b = 30 \mu m$, and thickness $t = 1.9 \mu m$. a) SEM of “T” beam bending prior to failure. b) Fracture surface after failure.

For silicon nitride we pick an arbitrary strength of $\sigma_f = 10$ GPa, modulus of $E = 385$ GPa, half thickness $c = 0.28$, inclination $\theta = 10^\circ$, and scale factor $n = 10$. Using equation (7) yields $L_a = 1.9 \mu m$.

Based on the above estimates, silicon cantilever “T” beams with dimensions of $L_a = 6.55 \mu m$, $w_a = 6.25 \mu m$, $L_b = 60 \mu m$, $w_b = 30 \mu m$, and thickness $t = 1.9 \mu m$ were fabricated and tested according to the above procedure. A deformed cantilever specimen is shown in Fig. 3a. The maximum rotation θ of region B was measured just prior to failure. Preliminary results indicate that the angle of rotation at failure is slightly greater than 20 degrees. A fracture surface is shown in Fig. 3b. The corresponding failure stress computed using equation (7) is $\sigma_f = 9.4$ GPa.

The same experiment was completed for silicon nitride with $L_a = 2.3 \mu m$, $w_a = 2.1 \mu m$, $L_b = 20 \mu m$, $w_b = 10 \mu m$, and thickness $t = 0.55 \mu m$. All of the tests failed at angles much greater than 20 degrees. Consequently, for the current set of results, the angle may be too large for the equations presented above. However, we know that the specimens fail at angles greater than 20 degrees. As a result we may choose 20 degrees as a lower limit to yield a conservative estimate of the strength. The corresponding failure stress for silicon nitride computed using equation (7) is $\sigma_f = 16.9$ GPa.

The larger than expected angles of rotation may be due to the shape of the membrane at the fixed end of region A. As shown in Fig. 3a, the base of region A is attached to the surrounding membrane, which was cut to the same width as region B. If the base membrane was left uncut, the stiffness would increase, and the specimen would fail at lower angles. In either case the important value of rotation is the relative difference between the base and end rotations of region A.

The above failure stress values are on the same order as those reported by Johansson et. al.,¹² but much greater than the values presented by Wilson et. al.⁶ This is consistent with the fracture theory that smaller volume results in fewer flaws and higher strengths. Here we have thicknesses less than one tenth of the thicknesses used by Wilson et. al.⁶ The coating material may also provide a small increase of the strength.¹²

Here we note that the base of region A is not placed at the edge of the membrane where it meets the bulk material thickness as was done in Ref. 6. The configuration presented herein eliminates the sharp corner and resulting stress concentration. This allows us to approximate the stresses fairly accurately with simple equations, rather than detailed three-dimensional finite element models. At this point the actual accuracy of equation (7) is unclear for large angles. Due to time constraints we were unable to validate this equation. However, in future work we will compare the equations to a detailed finite element model for large rotations.

2.4. Shutter Design, Analysis, and Testing

A schematic of a single shutter is shown in Fig. 1. The shutter is comprised of a 100 by 100 μm blade suspended on torsion bars extending the width of the blade. The torsion bars attach to the membrane of the full array of shutters at the ends. In operation the shutter blade is rotated vertically out of plane resulting in a 90 degree twist of each of

the torsion bars. The torsion bars must be sufficiently compliant to reliably twist without failing, but at the same time, sufficiently rigid to react the actuation forces described in Ref. 1.

Because the membrane material is brittle, it is desirable to eliminate stress concentrations and stress gradients where possible, and ensure that the maximum stresses are well below the failure strength. For the preliminary design presented herein, we use the minimum fracture strength as a first approximation for the allowable stress. As a result, we must maintain a large margin between the peak and allowable stresses due to the uncertainty introduced by this approximation. In future work, the uncertainty may be reduced by employing the Weibull probability distribution function.

Initially, the torsion elements may be sized using the torsion equations^{8,9}

$$\theta = \frac{TL}{KG} \quad \text{and} \quad T = \frac{\theta KG}{L}. \quad (8)$$

where θ is the twist angle about the long axis of the beam, T is the corresponding twisting moment, L is the length, K is a torsional stiffness constant, and G is the modulus of rigidity. For a rectangular cross section the torsional stiffness constant is expressed as

$$K = ab^3 \left[\frac{16}{3} - 3.36 \frac{b}{a} \left(1 - \frac{b^4}{12a^4} \right) \right] \quad (9)$$

and the maximum shear stress τ is

$$\max \tau = \frac{3T}{8ab^2} \left[1 + 0.6095 \frac{b}{a} + 0.8865 \left(\frac{b}{a} \right)^2 - 1.8023 \left(\frac{b}{a} \right)^3 + 0.9100 \left(\frac{b}{a} \right)^4 \right] \quad \text{for } a \geq b. \quad (10)$$

In equations (9) and (10), a is half the long edge of the rectangular section, and b is half the short edge.

The rotation of the shutter is a highly non-linear large deformation process, and the above equations are rooted in linear elastic theory. In order to validate the above equations for this problem, a non-linear finite element model of the shutter was developed in IntelliCAD.¹³ Various angles of rotation were applied to the shutter blade and the peak stresses were monitored. We observed that the peak stress in the torsion beams increased linearly with angle of rotation all the way through a rotation of 180 degrees. Consequently, the above expressions for peak stress in the torsion bars are satisfactory for the current application.

The silicon and silicon nitride membrane thicknesses are fixed at $1.9 \mu\text{m}$ and $0.55 \mu\text{m}$, respectively, in this study. However, our objective is to optimize the width w , and thickness t of the torsion beams. Rather than impose a stress τ and solve for w for a given t , we plot τ versus w and t for 90 degree rotation as shown in Figs. 4 and 5, respectively. The above figures show that the stress is less sensitive to increases in the longer side of the rectangular section, and is dominated by the length of the shorter side.

A detailed finite element model of the silicon shutter was developed using ANSYS, with membrane thickness $t = 1.9 \mu\text{m}$ and blade dimensions of $100 \mu\text{m}$ by $100 \mu\text{m}$. The torsion bar had length and width of $112 \mu\text{m}$ and $2 \mu\text{m}$, respectively. The “neck” region connecting the blade to the torsion bar was $3 \mu\text{m}$ by $8 \mu\text{m}$. For the material properties we used moduli $E = 176 \text{ GPa}$ and $G = 80 \text{ GPa}$ corresponding to the $\langle 110 \rangle$ direction, moduli $E = 130 \text{ GPa}$ and $G = 50 \text{ GPa}$ corresponding to the $\langle 100 \rangle$ direction, and Poisson’s ratios of $\nu = 0.279$ and $\nu = 0.064$, respectively. In this case the torsion bar section half width is $b = 1 \mu\text{m}$ and half height is $a = 0.95 \mu\text{m}$. The low aspect ratio between these values necessitates using brick elements in the model. We choose brick elements over beam elements to capture stress gradients in any direction.

The above finite element model predicted a peak maximum principal stress of 3.6 GPa for a 90 degree rotation, which is considerably lower than the fracture stress of 9.4 GPa determined in the previous section. However, for a 180 degree rotation, the predicted peak maximum principal stress is 7.4 GPa , which is relatively close to the strength, given the preliminary nature of the results. We assume that the state of stress in the torsion element is approximately pure torsion. For a state of pure torsion the maximum principal stress equals the maximum shear stress and can be compared directly to Figs. 4 and 5. For a 2 by 2 μm torsion bar the maximum shear stress from Fig. 4 is approximately 2.9 GPa , which is on the same order of the above finite element value.

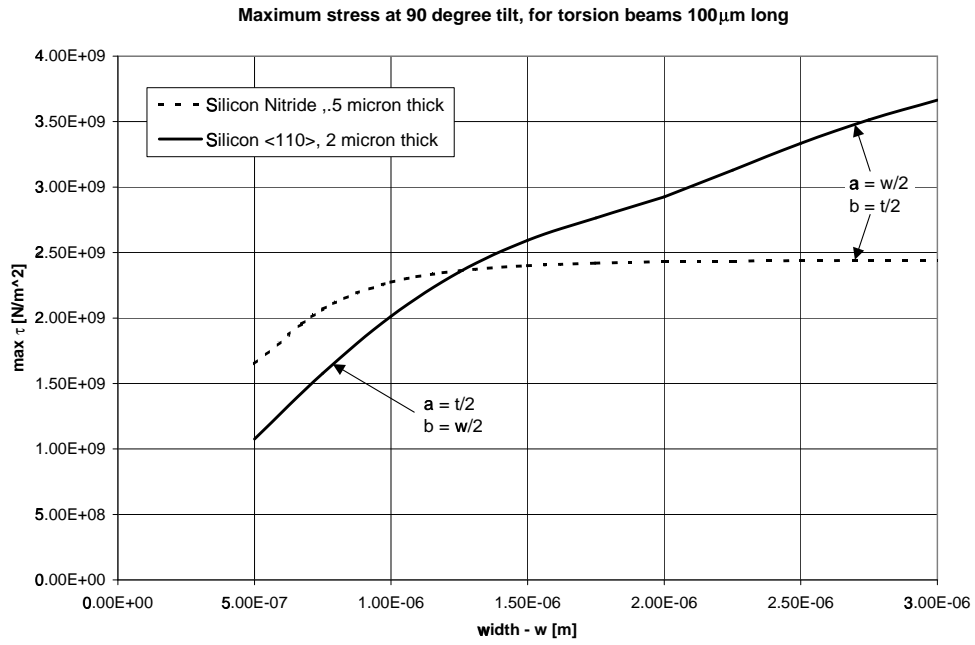


Figure 4. Maximum shear stress versus beam width governed by equation (10) for silicon and silicon nitride.

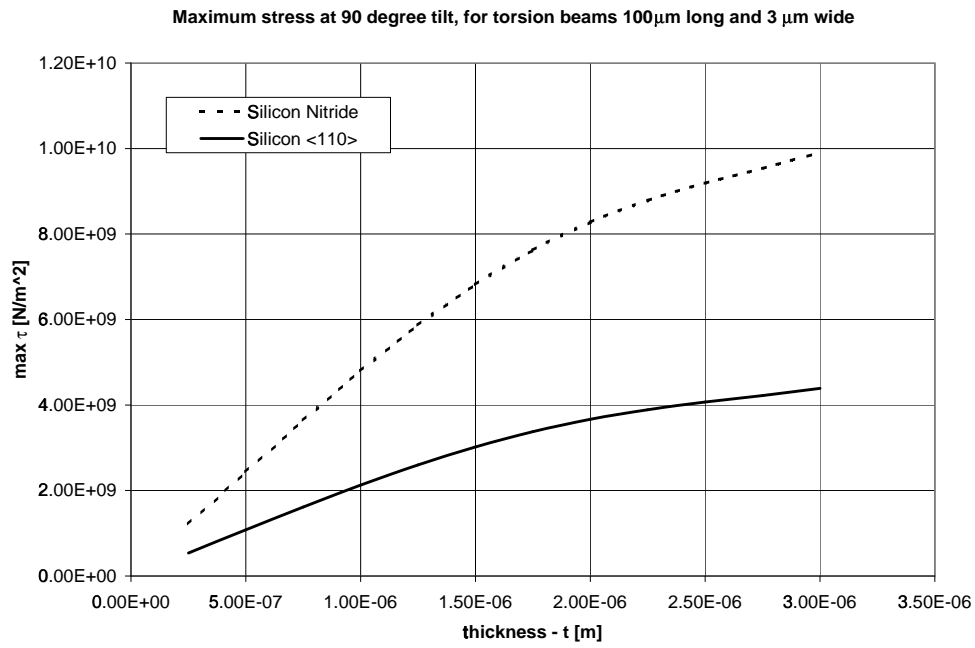


Figure 5. Maximum shear stress versus beam thickness governed by equation (10) for silicon and silicon nitride.

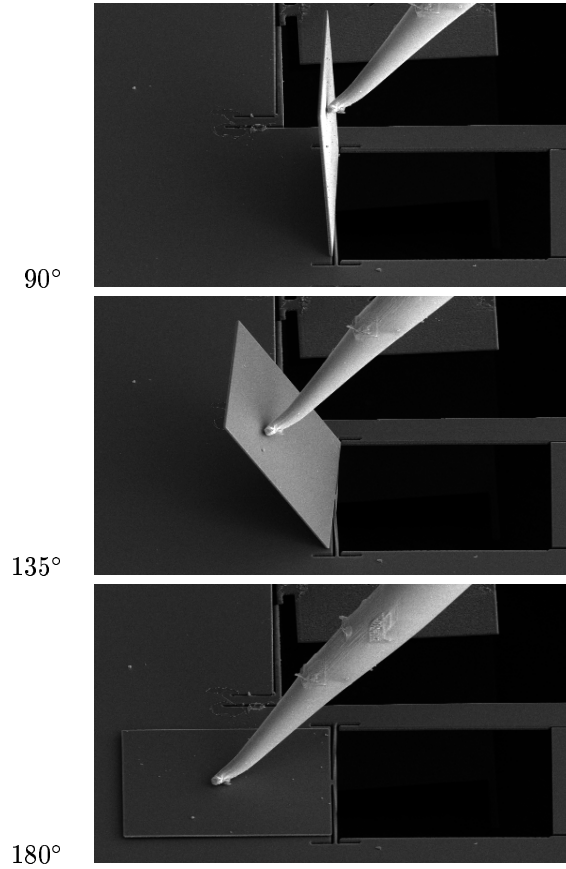


Figure 6. Micro-shutter rotated approximately 90, 135, and 180 degrees.

Shutters with the same dimensions were fabricated using the focused ion beam machine. The shutters were rotated through 90 degrees and subsequently 180 degrees using a needle. A rotated shutter is shown in Fig. 6. No failures were observed for a 90 degree rotation. A few shutters failed near the 180 degree rotation. In these cases, the torsion beams failed near the fixed end. In most cases there was no hysteresis. However, in one case the shutter returned to a slightly different position after it was rotated 180 degrees and released. In this case, no cracks were observed, however, there was most likely fracture initiation and the shutter was very near to catastrophic failure. These observations are strikingly consistent with the finite element and strength results.

Shutters with the same geometry, except for $t = 0.55 \mu m$, were fabricated and modeled using silicon nitride. The finite element model predicted a peak maximum principal stress of 2.3 GPa for a 90 degree rotation, and 4.6 GPa for a 180 degree rotation. Both of these stress values are significantly lower than the conservative value of 16.9 GPa determined in the previous section. In testing, these were noticeably more robust than those machined from silicon, which is consistent with the higher strength. For a torsion bar with $t = .5 \mu m$ and $w = 2 \mu m$, the maximum shear stress from Fig. 4 is approximately 2.4 GPa, which is very close to the above finite element value.

3. DISCUSSION

Each phase of the design process outlined herein is highly sensitive to the membrane thickness and cross sectional shape. Both bending and torsion are functions of the thickness to the 3rd or 4th power. In this work we assumed a rectangular cross section, but in fact the thickness varies across the width of most structures due to the rounded edge left by the focused ion beam. The thickness is relatively difficult to measure accurately. Consequently a small error in thickness is compounded by error in the cross sectional shape, which enters the equations through the area moment of inertia I . As mentioned above this is a critical source of error for tests that involve bending and torsion.

If we use the peak thickness of the section the models will tend to be more stiff than reality. In future work the torsion equations can be written for an elliptical cross section and used in conjunction with the rectangular section to establish upper and lower bounds.

Because the membranes are so thin we found it difficult to induce failure using the bending test. However, the design does have strong potential. In future work, the base membrane should be left intact, which will result in failures at lower angles of rotation. Switching to simple tensile tests may be preferable, however, the thinness of the specimens results in extremely small forces and displacements to failure, which may be difficult to measure.

While we have met the requirement that the shutters endure 90 degree rotation without failure, the torsion beams are very compliant. They tend to bow more than desirable when the rotation load is applied. This is due in part to the fact that the shutter actually sees combined loading during the rotation, both in the simple single shutter experiments and in the array operation. These aspects can be improved using Figs. 4 and 5 and through more detailed finite element modeling. These models can be correlated to the experiments by measuring the resonant frequency of the shutter, and adjusting and improving the model until the frequencies match.

While the shutter design presented herein experienced few failures in testing, more work needs to be done to quantify how reliable the shutters will be in service. If we test and there is no failure, we may have zero margin with no factor of safety. In service the device may be exposed to additional loads that drive stresses over the edge and result in failure. The most sound approach would be to experimentally determine the Weibull parameters and derive a highly reliable stress allowable. It may also be prudent to develop a torsion fracture test. While bending will tend to cause crack opening (Mode I and Mode II) failures, torsion may be dominated by Mode II and Mode III cracks. The processing could result in preferential flaws that may or may not affect the strengths for the different types of loading.

The operating temperature of the micro-shutter array will be 30K. The thermally induced mismatch stresses between the membrane and coating is not expected to result in failure because the coatings are thin. However, there may be problematic thermal mismatches between the arrays and the packaging. These effects will be considered in conjunction with the 90 degree rotation in future studies.

4. CONCLUSION

A preliminary design of the basic micro-shutter element used in a micro-shutter array has been completed. Initially, the test setup was validated by measuring the Young's modulus of micro-cantilever beams using a vibration test. The minimum fracture strength was determined using a bending test, and simplified beam equations. Beam deflection equations were used to size the torsion beams relative to the measured strengths. Micro-shutters were fabricated and tested. The shutters were found to sustain 90 degree rotations without failing. Silicon nitride was found to be more resistant to failure for the set of dimensions used in the study.

The micro-shutter finite element results appeared to be consistent with the preliminary strength data presented herein. While the approach is approximate, strong agreement was observed between the simplified equations, finite element models, and tests. As a result the simplified equations can be used to understand design trade-offs and are adequate to help guide the design. Once an initial design is selected based on these equations and tests, the structure can be simulated with detailed finite element analysis for further refinement and flight qualification analysis.

ACKNOWLEDGMENTS

This project was supported by a grant from NGST GSFC 98-01. The authors gratefully acknowledge Christine Allen from NASA/GSFC Code 553 for providing the back etched silicon wafers, and Tina Chen from Global Science and Technology for providing the silicon nitride membranes used in this work.

REFERENCES

1. S. Moseley, R. Fettig, A. Kutyrev, C. Bowers, R. Kimble, J. Orloff, and B. Woodgate, "Programmable 2-dimensional microshutter arrays," in *Micromachining and Microfabrication, Proceedings of SPIE* **3878**, Sept. 1999.
2. J.-A. Schweitz and F. Ericson, "Evaluation of mechanical materials properties by means of surface micromachined structures," *Sensors and Actuators* **74**, pp. 126-133, 1999.

3. W. Weibull, "A statistical distribution function of wide applicability," *J. Appl. Mech.* **18**, p. 293, 1951.
4. SAS IP, Inc., Canonsburg, PA, *ANSYS Version 5.4*, 1997.
5. F. Ericson and J.-A. Schweitz, "Micromechanical fracture strength of silicon," *J. Appl. Phys.* **68**, pp. 5840–5844, Sept. 1990.
6. C. Wilson, A. Ormeggi, and M. Narbutovskih, "Fracture testing of silicon microcantilever beams," *J. Appl. Phys.* **79**, pp. 2386–2393, Mar. 1996.
7. S. Johansson and J.-A. Schweitz, "Fracture testing of silicon microelements in situ in a scanning electron microscope," *J. Appl. Phys.* **63**, pp. 4799–4803, May 1988.
8. W. D. Pilkey, *Formulas for stress, strain, and structural matrices*, J. Wiley, New York, 1994.
9. W. C. Young, *Roark's Formulas for Stress and Strain*, McGraw-Hill, Inc., New York, 1989.
10. B. Bhushan and X. Li, "Micromechanical and tribological characterization of doped single-crystal silicon and polysilicon films for microelectromechanical systems," *J. Mater. Res.* **12**, pp. 54–63, Jan. 1997.
11. N. MacDonald, L. Chen, J. Yao, Z. Zhang, J. McMillan, D. Thomas, and K. Haselton, "Selective chemical vapor-deposition of tungsten for microelectromechanical structures," *Sensors and Actuators* **20**, pp. 123–133, Nov. 1989.
12. S. Johansson, F. Ericson, and J.-A. Schweitz, "Influence of surface coatings on elasticity, residual stresses, and fracture properties of silicon microelements," *J. Appl. Phys.* **65**, pp. 122–128, Jan. 1989.
13. IntelliSense Corporation, Wilmington, MA, *IntelliCAD*.